Convection-enhanced biopatterning with recirculation of hydrodynamically confined nanoliter volumes of reagents

Julien Autebert*, Julien F. Cors*, David P. Taylor and Govind. V. Kaigala

IBM Research-Zurich, Säumerstrasse 4, CH-8803 Rüschlikon, Switzerland.

* contributed equally to this work

Supporting Information

SI-1. Analyte consumption in a microchannel.

We consider deposition of immunoglobulin (IgG) on a deposition zone with a length of 100 µm within a 100 µm deep channel and a flow rate of 1 µl/min. IgGs in solution that flow over the deposition zone can find a binding partner within the deposition zone. This leads to formation of a depletion zone that extends to about 1.5 µm (based on Squires *et al.*[1]) of the 100 µm deep channel. All IgGs flowing through the remaining 98.5 µm of the channel depth are not available for the binding reaction at the surface and thus the overall usage of available analytes is well below 1.5%.

SI-2. Operation of the microfabricated MFP head for liquid recirculation.

We fabricated a glass/silicon head comprising hydrodynamic resistors, storage and mixing zones and fluidic vias for connection to the reservoirs (see Fig. S2). We used a hierarchical flow confinement, with the flow rates following three rules: both injections are identical, $Q_{i1} = Q_{i2}$; total aspiration is sufficiently high to ensure a stable HFC, $|Q_{a1} + Q_{a2}| = 3(Q_{i1} + Q_{i2})$; and dilution must be minimal, $Q_{i1} = |Q_{a2}|$. We observed a stable and well defined HFC (Fig. S2.b, state *1*). Upon switching the four pressures in the reservoirs, we observed a rapid (< 1 s) establishment of the HFC with reversed flow direction (see Fig. S2.b, state *2*).

Two serpentine zones, of 1 µl volume each, ensure in-head storage and homogenization of the processing liquid (see Fig S2.a.). Further reduction of this volume is feasible to the extent that the total volume of the recirculated liquid must be large compared to the fraction of processing liquid lost to the outer aspiration during switching, typically below 1 nl per cycle at a flow rate of 1 µl/min.

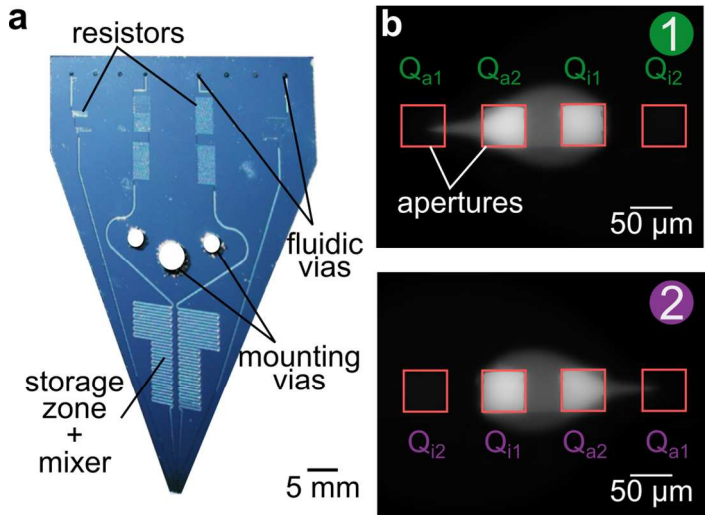

Figure S2. Microfabricated MFP head generating a hydrodynamic flow confinement. (**a**) MFP head with hydrodynamic resistors, two 1 µl storage zones, two mixers, fluidic vias, and mounting vias. (**b**) Micrographs of a hydrodynamic flow confinement between the apex and the surface (d = 30 µm). Switching from state *1* to state *2* occurs within 1 s.

SI-3. Diffusive transport between two laminar flows within the HFC.

For the evaluation of the velocity vector field between apex and surface, we assume that the fluid flow from and to the apertures of the MFP head can be described with the Hele-Shaw approximation. The apex-to-surface distance d is in the order of 10 µm, while the lateral dimension of the apex is in the range of 1 mm. Movement of liquid perpendicular to the apex is therefore significant up to a distance of approximately 10 µm from each aperture. In this model, we neglect any movement of liquid perpendicular to the apex and do a far field analysis by considering the apertures as line sources, stretching between the apex of the MFP and the surface.

Each source individually produces a radial field of liquid flow and is assumed as the center of a cylindrical coordinate system. The velocity vector field $\vec{u}(r,z)$ of liquid flow depends on the distance from the source r and the vertical position z between the apex and the surface. The surface is at $z = 0$, while the apex is at $z = d$. The net flow through a cylindrical boundary around the source has to equal the flow Q_s effected by the source:

$$Q_S = \int_0^h \int_0^{2\pi} \vec{u}(r,z) \cdot r d\theta dz \qquad \text{(S1)}$$

Integration and solving for the velocity vector field $\vec{u}(r,z)$ for the respective source leads to:

$$\vec{u}(\vec{r},z) = \frac{3Q_S}{\pi h^3|\vec{r}|}\cdot z(d-z)\vec{e}_r \tag{S2}$$

The magnitude of velocity varies in z-direction according to the classic parabolic flow profile. We therefore reduce the problem to two dimensions by averaging the velocity in the z-direction:

$$\overrightarrow{\langle u\rangle}(\vec{r}) = \frac{1}{h}\int_0^h \frac{3Q_S}{\pi d^3 r}\cdot z(d-z)\vec{e}_r\, dz = \frac{Q_S}{2\pi d|\vec{r}|}\vec{e}_r \tag{S3}$$

By shifting sources to positions $\vec{r}_i$ and superimposing their respective averaged velocity vector fields, the resulting velocity vector field $\vec{U}(r)$ for any arbitrary combination of sources can be evaluated as:

$$\vec{U}(\vec{r}) = \sum_{i=1}^{n} \frac{Q_{S,i}\cdot(\vec{r}-\vec{r}_i)}{2\pi d\cdot|(\vec{r}-\vec{r}_i)|^2} \tag{S4}$$

The vector field $\vec{U}(r)$ contains the 2D information of liquid flow paths in the entire domain between the apex and the surface. The geometrical properties of potentially resulting HFC, such as size, shape and footprint area can be evaluated on the basis of this vector field.

In a single HFC, dilution of the processing liquid is driven primarily by its aspiration together with the surrounding liquid. In the hierarchical HFC, since $Q_{i1} = |Q_{a2}|$ dilution is solely due to diffusion of analytes from the processing liquid to the shaping liquid and is therefore limited. For efficient recirculation of the processing liquid, this loss of analytes should however be minimized. We developed a model to investigate the dilution γ of the processing liquid as a function of two key parameters, namely the apex-to-surface distance d and the flow rate of the processing liquid Q_{i1}.

We apply the advection-diffusion equation (S5) to study the transport of analytes. Here, v_χ and v_ρ denote the tangential and perpendicular components of the flow velocity.

$$\frac{\partial c}{\partial t} + v_\chi\frac{\partial c}{\partial \chi} + v_\rho\frac{\partial c}{\partial \rho} = D\cdot\left(\frac{\partial^2 c}{\partial \chi^2} + \frac{\partial^2 c}{\partial \rho^2}\right) \tag{S5}$$

The velocity field of liquid flow between the apex and the surface as well as the boundary conditions for concentration are static, therefore equation (S5) can be analyzed in steady-state. As $v_\rho = 0$ and $\frac{\partial^2 y}{\partial \rho^2} \gg \frac{\partial^2 c}{\partial \chi^2}$ equation (S5) becomes:

$$\frac{\partial c}{\partial \chi} = \frac{D}{\hat{v}_\chi}\cdot\frac{\partial^2 c}{\partial \rho^2} \tag{S6}$$

where $\hat{v}_\chi = \frac{1}{\chi}\int_0^\chi \hat{v}(u)du$ is the average tangential velocity along the interface up to a position χ along the interface. Since we consider the initial concentration profile being a Heaviside step function, equation (S6) is solved by:

$$c(\chi,\rho) = c_0 \cdot \left(\frac{1}{2} + \frac{1}{2} \cdot \mathrm{erf}\left(-\frac{\sqrt{\hat{v}_\chi} \cdot \rho}{\sqrt{4D \cdot \chi}}\right)\right) \tag{S7}$$

The flux $J(\chi)$ of analytes across the interface at a specific point χ along the interface is given by the gradient of the concentration in direction of ρ at χ:

$$J(\chi) = -D \cdot \frac{\partial c(\chi,0)}{\partial \rho} = c_0 \cdot \sqrt{\frac{D \cdot \hat{v}_\chi}{4\pi \cdot \chi}} \tag{S8}$$

To obtain the rate $\partial n_D/\partial t$ of analytes diffusing accross the interface, we integrate $J(\chi)$ along one-half of the interface and account for the apex-to-surface distance d, Avogadro's number N and a factor two for symmetry:

$$\frac{\partial n_D}{\partial t} = 2d \cdot N \cdot c_0 \cdot \int_0^{\chi_{max}} \sqrt{\frac{D \cdot \hat{v}_\chi}{4\pi \cdot u}}\, du \tag{S9}$$

The injection flow rate of processing liquid, Q_{i1}, defines the total rate of analytes transported through the confined liquids that can be evaluated as $\partial n_{in}/\partial t = N \cdot c_0 \cdot Q_{i1}$.

The dilution γ is expressed as the ratio between the rate of analytes diffusing from the processing liquid into the shaping liquid and the total rate of analytes transported through the confined liquids:

$$\gamma = \left.\frac{\partial n_D}{\partial t}\right/\frac{\partial n_{in}}{\partial t} = \frac{2d}{Q_{i1}} \int_0^{\chi_{max}} \sqrt{\frac{D \cdot \hat{v}_\chi}{4\pi \cdot u}}\, du \tag{S10}$$

Experimental validation:

To obtain a numerical value for γ, we developed a Matlab routine to calculate $\hat{v}_\chi$ for any position χ along the interface and to numerically evaluate the integral in equation (10). Theoretical values for γ are presented and compared to experimental dilution values in the following section.

The analyte concentration in the processing liquid will reduce for each circulation cycle. To experimentally measure this reduction in concentration, we recirculated a fluorescent dye (Rhodamine B) back and forth (cycles) and observed the drop in fluorescence. Using the hierarchical HFC with an injection flow rate Q_{i1} = 1 µl/min, we measured an average drop in fluorescence of 10.67 ± 1.05 % per cycle, corresponding to 36.2 % of the initial concentration after 10 cycles (Fig. S3.a, black). For a second injection flow rate, Q_{i1} = 2 µl/min, the fluorescence reduces by 4.75 ± 0.38 % per cycle, which corresponds to 64.5 % of the initial concentration after 10 cycles (Fig. S3.a, red). In comparison, the use of a single flow confinement resulted in a fluorescence reduction of 66 % after only one cycle, and a concentration as low as 0.09 % after 10 cycles (Fig S3.a, dashed line). These results suggests that during

recirculation the hierarchical HFC has the significant advantage of minimizing the dilution of the processing liquid compared with single HFC.

We also investigated the dilution of the processing liquid as a function of d for flow rates Q_{i1} =1, 2 and 3 µl/min, which are commonly used when operating the MFP (Fig. S3.b) and made two important observations. First, dilution in the inner flow confinement increases with the apex-to-surface distance. Indeed, when d increases, the boundary surface between the inner and outer flow confinements increases. In addition, for a given flow rate, the apex-to-surface distance will have an impact on the flow velocity at the interface, and therefore on the amount of analytes that can diffuse through the boundary prior to being reaspirated. Second, dilution is lower at higher flow rates: an increase of the flow rate results in an increase of the flow velocity along the boundary. This implies that both the net flux of analytes diffusing to the surface, $\partial n_D/\partial t$, and the total amount of analytes injected through the aperture $\partial n_{in}/\partial t$ will increase, the former less than the latter, resulting in increased dilution as $\gamma = \left.\frac{\partial n_D}{\partial t}\right/\frac{\partial n_{in}}{\partial t}$.

Both the experimental results and the analytical model exhibit similar trends and dilution values. As an example, for Q_3 = 3 µl/min, we used our analytical model to calculate the dilution of 4.11 % and measured a dilution of 4.24 ± 0.78 % for an apex-to-surface distance d = 10 µm. This excellent correlation between experiments and theory suggest that dilution is indeed primarily driven by diffusion at the liquid-liquid interface. At low flow rates, for example, Q_1 = 1 µl/min and for distances below 20 µm, we observed a minor discrepancy between the model and experimental results. This is potentially due to the change of the three-dimensional shape of the HFC that we noticed experimentally and not accounted for in our model.

Therefore, according to both analytical and experimental dilution values, efficient recirculation is favored at higher flow rates and when the head is in close proximity of the surface. We note however that the flow rate will influence the amount of processing liquid used per circulation cycle. This implies that for a finite volume of processing liquid, there is a trade-off between the flow rate of the processing liquid and the number of circulation cycles per minute for a given volume of processing liquid. Depending on the application, parameters such as apex-to-surface distance and flow rates need to be adjusted to ensure proper surface processing and minimal loss of processing liquid.

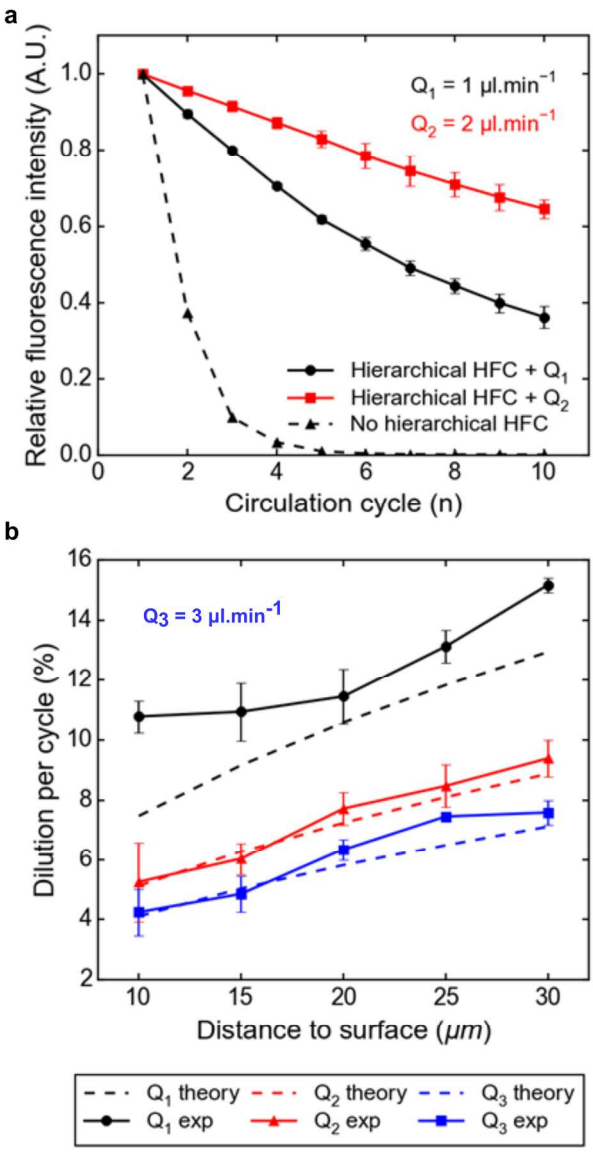

Figure S3. The dilution of the processing liquid in the inner HFC depends on the apex-to-surface distance and the flow rates. (**a**) For a fixed apex-to-surface distance (d = 20 µm), fluorescence measurements (n = 5) of the processing liquid show the dilution at each circulation cycle for different flow rates $Q_{a2} = Q_{i1}$ = 1 and 2 µl/min. (**b**) Comparison of the dilution per circulation cycle between theory and experiments for three flow rates $Q_{a2} = Q_{i1}$ = 1, 2 and 3 µl/min (n = 5).

SI-4. Deposition of analytes on a surface using the MFP.

Binding of secondary antibodies to the surface results in the formation of a depletion zone within the HFC. This depletion zone significantly limits the flux of antibodies to the surface and is therefore of interest in this analysis. For quantitative description of the influence of the depletion zone on the transport of analyte to the surface, we adapt an analytical approach summarized by Squires *et al.*[1]. The "global" Péclet number Pe_g is a measure for the size of the depletion zone relative to the geometrical boundaries of the HFC and is evaluated as:

$$Pe_g = \frac{Q_{i1}}{D_{Ig} \cdot W_{HFC}} \approx 2 \cdot 10^3 \tag{S11}$$

where W_{HFC} is the maximum width of the HFC footprint, Q_{i1} is the imposed flow rate in the inner HFC and $D_{Ig} = 3.9 * 10^{-7}\ cm^2/s$ (see ref.[2]) is the diffusion coefficient of the antibodies to be deposited. We assume an inner HFC with $L_{HFC} = W_{HFC} = 250\ \mu m$, an injection and aspiration flow rate $Q_{i1} = 1\ \mu l/min$. Hence, for flow conditions to be expected during MFP operation, $Pe_g \gg 100$ and thus the depletion zone is small compared to the size of the HFC. The "local" Péclet number Pe_l is a measure for the thickness of the depletion zone relative to the length of the deposition area and is given by:

$$Pe_l = 6Pe_g \cdot \left(\frac{L_{HFC}}{d}\right)^2 \approx 2 \cdot 10^6 \tag{S12}$$

As $Pe_l \gg 100$, the thickness of the depletion zone is small compared to the length of the HFC footprint. While size and shape of the depletion zone obeys the advective transport of analyte, solely diffusive transport enables the analyte to pass through the depletion zone and to eventually interact with the surface. With Pe_g and Pe_l being large, the dimensionless flux $\mathcal{F}$ of analyte molecules through a thin depletion zone as described above can be calculated numerically[1,3] as:

$$\mathcal{F} \approx 0.81 \cdot {Pe_l}^{\frac{1}{3}} + 0.71 \cdot {Pe_l}^{-\frac{1}{6}} - 0.2 \cdot {Pe_l}^{-\frac{1}{3}} \approx 95 \tag{S13}$$

After estimating the flux of analyte to the surface, we now focus on the interaction between the primary and secondary antibodies on the surface. We assume this interaction to obey first order Langmuir kinetics. The Damköhler number Da represents the ratio between the consumption of analyte on the surface and transport rate of analytes. For $Da \gg 1$, the deposition process is transport limited, wheras for $Da \ll 1$, the process is reaction limited. For the assumed system geometry, flow conditions and the chosen analyte receptor system, Da can be evaluated as follows

$$Da = \frac{k_{on} \cdot b_m \cdot L_{HFC}}{D_{Ig} \cdot \mathcal{F} \cdot N} \approx 2.8 \tag{S14}$$

We used a set of parameters typical of MFP operation: a surface area of 250 µm × 250 µm presenting binding sites at a density of 18000 sites/µm^2 and a processing liquid containing an antibody solution. The molar weight of the dispersed antibodies is 150000 g/mol and their diffusion coefficient is estimated to be 3.8×10^{-7} cm^2/s. For the binding reaction, we presume first order Langmuir kinetics with $k_{on} = 10^6$ l/mol·s and $k_{off} = 10^{-3}$ s^{-1}. (see ref[3])

Assuming first order Langmuir kinetics and accounting for the diffusion-limited transport to the surface, the dynamics of the surface density of bound analytes $b_{MFP}(t)$ can therefore be described by:

$$b_{MFP}(t) = \frac{k_{on} c_0 b_m}{k_{on} c_0 + k_{off}} \left(1 - e^{-\frac{k_{on} c_0 + k_{off}}{Da} \cdot t}\right) \tag{S15}$$

where the retarding effect of the limited flux through the depletion zone is accounted for by the factor Da^{-1}.

When the processing liquid is pipetted onto a surface coated with a primary antibody, the growth of the depletion zone is not counterbalanced by advective transport and the flux of analytes to the surface reduces continuously (see S4). Consequently, the Damköhler number depends on time and thus the surface density of bound analytes for pipette-based deposition $b_{\mathrm{Pipette}}(t)$ can be approximated as:

$$b_{Pipette}(t) = \frac{k_{on} c_0 b_m}{k_{on} c_0 + k_{off}} \left(1 - e^{-\frac{(k_{on} c_0 + k_{off}) \cdot 40 D_{Ig} \cdot N}{k_{on} b_m L_{HFC}} \cdot \sqrt{t}}\right) \tag{S16}$$

The metric $\varepsilon(t)$ that quantifies the benefit of convective transport as compared to diffusion-driven transport for surface biopatterning. The ratio $\varepsilon(t)$ of analyte bound with the MFP compared with that of pipette deposition can be evaluated as:

$$\varepsilon(t) = \frac{\left(1 - e^{-\frac{k_{on} c_0 + k_{off}}{Da} \cdot t}\right)}{\left(1 - e^{-\frac{(k_{on} c_0 + k_{off}) \cdot 40 D_{Ig} \cdot N}{k_{on} b_m L_{HFC}} \cdot \sqrt{t}}\right)} \tag{S17}$$

SI-5. Matlab code for estimation of flow velocity fields.

The Matlab code generates the flow velocity field and diffusion profile described in the Results section. The code is contained in the function "Diffusion," which expects following input parameters: Outer injection flow rate [µl/min], inner injection flow rate [µl/min], inner aspiration flow rate [µl/min], outer aspiration flow rate [µl/min], diffusion coefficient [µm^2/s], apex-to-surface distance [µm]. The output of

the function is the percentual dilution of reaspirated processing liquid. The function returns results representative for the discussion in the main paper when called by following command:

Dilution = Diffusion(1,1,1,5,4.5*1E2,20)

The function will also plot the following figures in order to emphasize key aspects of the analysis.

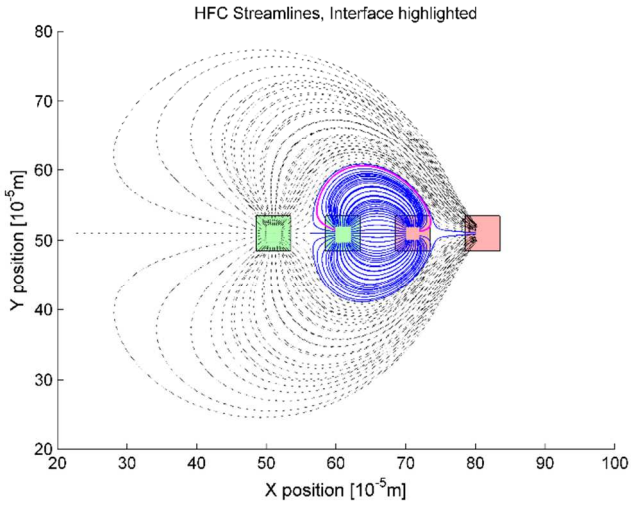

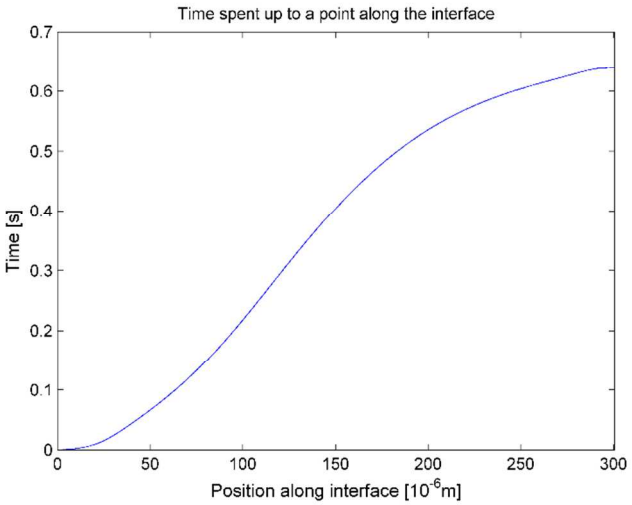

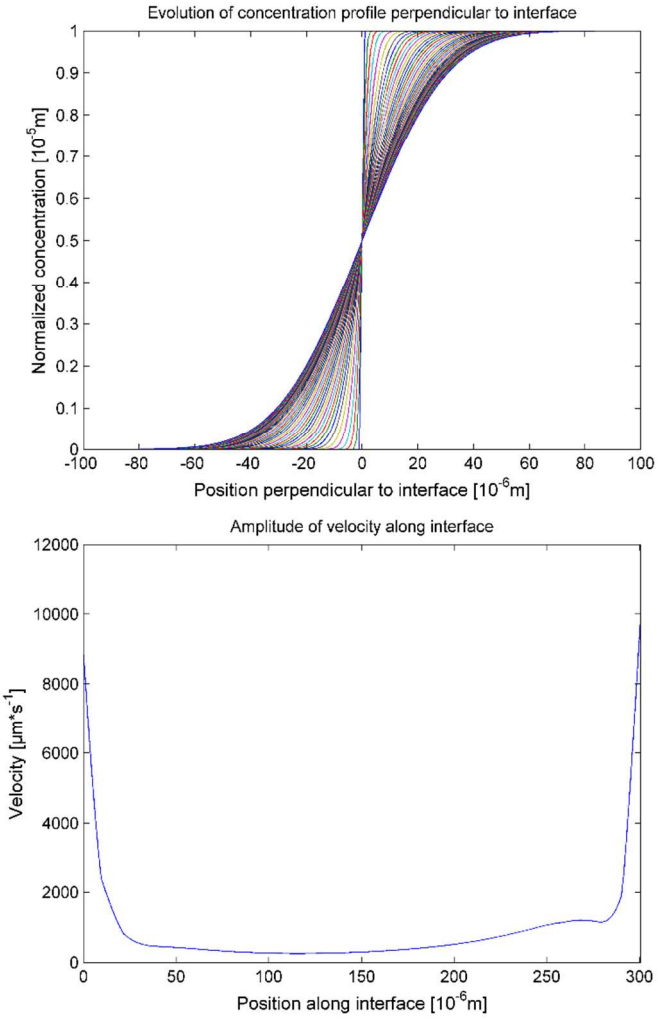

References:

1. Squires, T. M., Messinger, R. J. & Manalis, S. R. Making it stick: convection, reaction and diffusion in surface-based biosensors. *Nat. Biotechnol.* **26,** 417–426 (2008).

2. Jøssang, T., Feder, J. & Rosenqvist, E. Photon correlation spectroscopy of human IgG. *J. Protein Chem.* **7,** 165–71 (1988).

3. Newman, J. & Thomas-Alyea, K. E. *Electrochemical Systems*. (John Wiley & Sons, 2004).